Stable Hydrazone-Linked Covalent Organic Frameworks Containing *O,N,O'*-Chelating Sites for Fe(III) Detection in Water

Gui Chen,† Hai-Hang Lan,† Song-Liang Cai,*,†,‡ Bing Sun,‡,§ Xin-Le Li,‡ Zi-Hao He,† Sheng-Run Zheng,† Jun Fan,† Yi Liu*,‡ and Wei-Guang Zhang*,†

†School of Chemistry and Environment, South China Normal University, Guangzhou 510006, P. R. China

‡The Molecular Foundry, Lawrence Berkeley National Laboratory, Berkeley, California 94720, United States

§School of Science, China University of Geosciences (Beijing), Beijing 100083, P. R. China

KEYWORDS: Covalent Organic Frameworks, Functional Chelating Sites, Hydrazone-Linked COF, Iron(III) Selective Fluorescent Probe, Stable Luminescent COF.

ABSTRACT: Two stable crystalline hydrazone-linked covalent organic frameworks (COFs) (**Bth-Dha** and **Bth-Dma**) containing functional *O,N,O'*-chelating sites have been designed and successfully synthesized by the Schiff-base condensation reactions between benzene-1,3,5-tricarbohydrazide (**Bth**) and 2,5-dihydroxyterephthalaldehyde (**Dha**) or 2,5-dimethoxyterephthal-aldehyde (**Dma**), respectively. **Bth-Dma** exhibits strong fluorescence in the solid state and in aqueous dispersions, while no fluorescence can be observed for **Bth-Dha**. Interestingly, the as-synthesized **Bth-Dma** can be used as a turn-off fluorescence sensor for Fe(III) ion in aqueous solution with outstanding selectivity and sensitivity. The recognition process can be attributed to the coordination interaction between Fe(III) ion and the *O,N,O'*-chelating sites in the pore wall of **Bth-Dma** COF, as verified by X-ray photoelectron spectroscopy and ^{1}H NMR spectroscopy. To the best of our knowledge, this is the first report on the rational design of luminescent COF with predesigned *O,N,O'*-chelating sites as a fluorescence sensor for highly selective and sensitive metal ion detection. This work may pave the way for designing luminescent COF sensors with functional binding sites for detecting specific metal ions.

INTRODUCTION

Covalent organic frameworks (COFs), constructed by the linkage of molecular building units *via* strong covalent bonds, represent a new type of fascinating porous crystalline organic polymers with well-defined two-dimensional (2D) or three-dimensional (3D) networks.[1] The rational design and targeted synthesis of COFs have attracted widespread attention over the past decade owing to their peculiar properties such as low mass density, high stability, large specific surface area and controllable pore structure.[2-5] Thus, COFs have been exploited in a plethora of applications such as gas adsorption,[6-8] drug delivery,[9-11] heterogeneous catalysis[12-14] and proton conduction,[15-17] to name a few. Recently, COFs with responsive fluorescent properties have emerged as a promising class of materials for sensing applications.[18] COF's feature of holding many copies of identical binding sites within one extended framework sets the stage for high sensitivity — when a single binding event occurs on one of the binding sites, the signal can be effectively transduced through the framework and amplified. However, robust fluorescent COFs for chemical sensing still remain under-developed, especially when compared to their counterparts, metal-organic frameworks (MOFs).[19,20] Indeed, only a few crystalline COFs have been employed as fluorescent chemsensors for the detection of nitroaromatic explosives,[21-23] metal cations[24-26] and biomolecules.[27]

Iron ion is one of the most important metal ions for human beings and other living organisms, and has a great impact on biochemical processes and biological systems.[28] The detection and quantification of Fe(III) ion are extremely essential for living organisms since either the deficiency or overload of Fe(III) ion can result in many physiological disorders.[29] Consequently, the development of new luminescent framework materials that can be used for effective detection of Fe(III) is of great significance. In recent years, extensive efforts have been dedicated to the design and construction of functional luminescent MOF-based materials for detecting Fe(III) ion.[19,20] Particularly, MOF structures that contain potential Lewis base sites have been realized to detect Fe(III) ion with enhanced sensing ability.[30,31] On the contrary, fluorescent COF-based chemsensors bearing functional chelating sites for the detection of Fe(III) is extremely scarce, and undoubtedly highly desired.

It has been reported that Fe(III) forms a strong coordination complex with salicylaldehyde benzoyl hydrazone (**SBH**) through *O,N,O'*-Fe(III)-chelating, as evidenced by single-crystal X-ray diffraction analysis (Scheme S1a).[32] Interestingly, hydrothermal reaction of *o*-methoxybenzaldehyde benzoyl hydrazone (**MBH**)

with Fe(III) ion gave rise to a new Fe(III) complex, in which Fe(III) coordinates with two **SBH** ligands that are generated through *in situ* demethylation (Scheme S1b and Table S1). Given the similar binding motif between *O*,*N*,*O'*-chelating ligand and Fe(III) center from both **SBH** and **MBH**, introducing *O*,*N*,*O'*-chelating units into COFs system should provide recognition sites for specific binding of Fe(III). This rationale leads us to design and synthesize two highly stable hydrazone-linked COFs (**Bth-Dha** and **Bth-Dma**) with the above-mentioned chelating sites through the condensation reactions of benzene-1,3,5-tricarbohydrazide (**Bth**) with 2,5-dihydroxyterephthalaldehyde (**Dha**) or 2,5-dimethoxyterephthalaldehyde (**Dma**) under solvothermal conditions (Scheme 1). Both COFs possess good crystallinity and exhibit outstanding chemical stability towards different solvents. Although **Bth-Dha** is almost non-emissive, **Bth-Dma** displays intense fluorescence both in the solid state and in aqueous dispersion. The emission property of **Bth-Dma** COF is very sensitive and selective to Fe(III) ion over other metal ions in aqueous solution owning to a fluorescence quenching effect, making it a promising fluorescence probe for Fe(III) ion. X-ray photoelectron spectroscopy (XPS) and ^{1}H NMR spectroscopic studies indicate that the strong coordination interaction between Fe(III) ion and the predesigned *O*,*N*,*O'*-chelating sites in the pore wall of **Bth-Dma** are responsible for the selective fluorescence quenching.

EXPERIMENTAL

Materials and Measurements: Benzene-1,3,5-tricarbohydrazide (**Bth**) was prepared according to the literature method.[33] 2,5-dihydroxyterephthalaldehyde (**Dha**) and 2,5-dimethoxyterephthalaldehyde (**Dma**) were purchased from Beijing Huawei Ruike Chemical Co. Ltd. (China). Other materials were reagent grade obtained from commercial sources and used directly without further purification. Liquid proton and carbon nuclear magnetic resonance (^{1}H-NMR and ^{13}C-NMR) spectra were recorded on a Varian 400 (400 MHz) spectrometer at ambient temperature; the chemical shifts were referenced to TMS in the solvent signal in d_6-DMSO. Solid-state nuclear magnetic resonance (SSNMR) spectrum was performed on an Agilent-NMR-vnmrs 600 spectrometer (Agilent Technologies, Santa Clara, CA, USA) at ambient pressure. LC-MS was conducted employing an Agilent LC-MS equipment. Fourier transform infrared spectra (FT-IR) were acquired on a Spectrum Two FT-IR spectrometer (PerkinElmer, Germany) in the scope of 4000–500 cm^{-1} by using KBr pellets. Powder X-ray diffraction (PXRD) patterns were measured on a Japanese Science Ultima IV X-ray Powder Diffractometer operating at 40 mA and 40 kV using Cu Kα radiation in a 2θ range of 2-40° at room temperature. Thermogravimetric analysis (TGA) was carried out utilizing a Germany Benz TG 209 F3 Thermogravimetric Analyzer at a heating rate of 10 ^{o}C/min under air atmosphere. Nitrogen adsorption-desorption isotherms were measured at 77 K using an American Mike ASAP 2020 Plus HD88 surface area and porosity analyzer. Scanning electron microscopy (SEM) images were performed on a ZEISS Gemini 500 Scanning Electron Microscope. The fluorescence spectra were recorded on a Hitachi F-4600 Fluorescence Spectrometer (Hitachi, Japan) with a PMT voltage being 800 V and a scan speed being 1200 nm/min, and the slit width for both excitation and emission was set to 10 nm. UV-vis spectra were carried out on a Shimadzu UV-2550 spectrophotometer equipped with a Labsphere diffuse reflectance accessory. Particle-size distributions were measured using a Dynamic Light Scattering (DLS) spectrometer (Malvern Mastersizer 3000). The X-ray photoelectron spectroscopy (XPS) was observed on a Thermo Fisher Scientific K-Alpha+ spectrometer with Al Kα X-ray source.

Synthesis of the model compound Tmt: Benzene-1,3,5-tricarbohydrazide (**Bth**, 50 mg, 0.20 mmol) was dispersed in methanol (10 mL), and then 2-methoxybenzaldehyde (272 mg, 2.0 mmol) was added. The reaction mixture was heated at refluxed for 48 h under argon atmosphere. The formed precipitate was filtered, washed with methanol three times and dried under vacuum. The crude product could be purified by recrystallization from DMSO to afford **Tmt** as a white solid (99 mg, 82% yield). IR (KBr pellet, cm^{-1}): 3624w, 3193w, 3038m, 2837w, 1670s, 1601s, 1549m, 1488w, 1465w, 1438w, 1357w, 1292w, 1255s, 1177w, 1163w, 1111w, 1069w, 1047w, 1024w, 964w, 860w, 788w, 755m, 730w, 686w, 583w, 519w. ^{1}HNMR (DMSO-d_6, 298 K, 400 MHz): δ = 12.21 (s, 3H), 8.91 (s, 3H), 8.70 (s, 3H), 7.95 (d, J = 7.4 Hz, 3H), 7.54 – 7.43 (m, 3H), 7.16 (d, J = 8.4 Hz, 3H), 7.08 (t, J = 7.5 Hz, 3H), 3.91 (s, 9H). ^{13}C NMR (DMSO-d_6, 298 K, 100 MHz): δ = 162.3, 158.4, 144.5, 134.5, 132.3, 130.3, 126.1, 122.7, 121.3, 112.4, 56.3. MS (LC-MS) for $C_{33}H_{30}N_6O_6$ (calcd. 606.22): m/z = 605.16 [M − H]$^-$.

Scheme 1. Schematic illustration of the designed syntheses of **Bth-Dha** and **Bth-Dma** COFs, as well as the model compound **Tmt** containing functional *O*,*N*,*O'*-chelating sites.

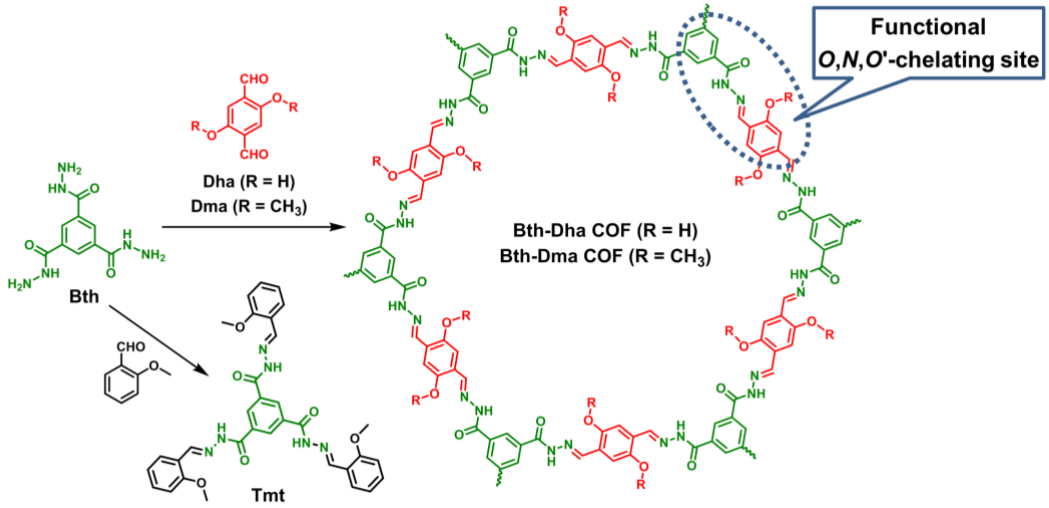

Synthesis of Bth-Dha COF: A mixture of benzene-1,3,5-tricarbohydrazide (**Bth**, 5.0 mg, 0.02 mmol), 2,5-dihydroxyterephthalaldehyde (**Dha**, 5.0 mg, 0.03 mmol), 1,4-dioxane/mesitylene (3:2, 1.0 mL) in a 10 mL vial was sonicated for 5 min, then 0.1 mL of acetic acid solution (6 M) was added. The reaction mixture was bubbled with argon for several minutes, after which the vial was rapidly sealed and placed in an oven to heat at 120° C for 5 days. The formed precipitate was collected by filtration, washed successively with 1,4-dioxane, anhydrous THF, and anhydrous acetone and dried under vacuum to produce a brown solid of **Bth-Dha** COF (8.1 mg, 91%). IR (KBr pellet, cm^{-1}): 3300m, 3190w, 3153w, 1657s, 1615m, 1547m, 1513s, 1437w, 1383w, 1329w, 1304w, 1256w, 1158w, 1006w, 961w, 915w, 874w, 844w, 824w, 803w, 734m, 679w, 622w, 602w. PXRD (2 theta): 3.4°, 5.9°, 9.0°, 26.8°.

Synthesis of Bth-Dma COF: Bth-Dma COF was prepared by a similar method as that used for **Bth-Dha**, except that **Dha** was replaced by the monomer of 2,5-dimethoxyterephthalaldehyde (**Dma**, 5.8 mg, 0.03 mmol), and 1,4-dioxane/mesitylene (3:2, 1.0 mL) was replaced by 1,4-dioxane/mesitylene (1:1, 1.0 mL). A yellow solid of **Bth-Dma** COF (9.1 mg, 93%) was obtained by filtration, washed with 1,4-dioxane, anhydrous THF, and anhydrous acetone, respectively, and dried under vacuum. IR (KBr pellet, cm^{-1}): 3747w, 3238w, 3064w, 2945w, 1663w, 1596w, 1552m, 1495w, 1466w, 1412s, 1361m, 1257s, 1213m, 1170w, 1111w, 1076w, 1036m, 1002w, 874w, 798w, 778w, 735w, 696w, 630w, 536w, 470w. PXRD (2 theta): 3.4°, 5.8°, 6.9°, 9.0°, 26.0°.

Sensing experiment of Bth-Dma COF towards metal ion: Stock solution of **Bth-Dma** COF (6 mg / L) was prepared by dispersing fine powder of **Bth-Dma** COF in water. The mixed solution was sonicated for a couple of hours to produce homogeneous suspension and used for luminescent measurements. The sensing experiments were performed by adding 1 mL aqueous solutions of chloride metal salts (NaCl, KCl, $MgCl_2$, $BaCl_2$, $CaCl_2$, $AlCl_3$, $MnCl_2$, $ZnCl_2$, $LaCl_3$, $GdCl_3$, $CoCl_2$, $NdCl_3$, $NiCl_2$, FeCl2, $CuCl_2$ and $FeCl_3$) at specific concentrations into 1 mL **Bth-Dma** COF suspension at room temperature and collecting the luminescence data immediately. All the emission spectra of **Bth-Dma** COF suspensions before and after the addition of metal ions were recorded from 450 to 700 nm upon excitation at 393 nm. The fluorescence quenching efficiency was estimated employing Stern–Volmer equation, $I_0/I = K_{SV}[M] + 1$, in which I and I_0 are the luminescence intensity of **Bth-Dma** COF with and without addition of Fe^{3+} cation, respectively, K_{SV} represents the quenching constant and [M] is the concentration of Fe^{3+} cation.

RESULTS AND DISCUSSION

The syntheses of the targeted **Bth-Dha** and **Bth-Dma** COFs were carried out under solvothermal conditions. Briefly, condensation reactions of **Bth** with **Dha** or **Dma** by employing mesitylene/1,4-dioxane as the cosolvents and 6 M acetic acid solution as the catalyst result in the production of **Bth-Dha** and **Bth-Dma** COFs in good yields. Moreover, in order to offer better insight into the structure and Fe(III) binding behavior of **Bth-Dma** COF, a hydrazone-linked model compound termed **Tmt** was also prepared (Scheme 1). Powder X-ray diffraction (PXRD) measurement was conducted to evaluate the crystallinity of the **Bth-Dha** and **Bth-Dma** COFs. As illustrated in Figure 1, PXRD patterns of both COFs present a strong diffraction peak at about 3.4°, which can be attributed to the reflection from the (100) facet. Besides, the additional weak peaks centered at 2θ = 5.9, 9.0 and 26.8° can be found for **Bth-Dha** COF, while those appeared at 2θ = 5.8, 6.9, 9.0 and 26.0° are observed for **Bth-Dma** COF. The last broad peak in both the PXRD patterns of **Bth-Dha** and **Bth-Dma** is assignable to the (001) facet. For the purpose of estimating the crystalline structures of these two COFs, plausible 2D layered structures with eclipsed AA (*P6/m* space group for **Bth-Dha**, Figure 1b and Table S2; *P6* space group for **Bth-Dma**, Figure 1e and Table S4) and staggered AB ($P6_3/m$ space group for **Bth-Dha,** Figure 1c and Table S3; $P6_3$ space group for **Bth-Dma**, Figure 1f and Table S5) stacking were modeled utilizing *Materials Studio* software. As described in Figure 1a and Figure 1d, the experimental PXRD patterns of both **Bth-Dha** and **Bth-Dma** match better with the corresponding simulated patterns generated from the eclipsed AA structures rather than the staggered AB ones, and is consistent with a very recent report of an identical **Bth-Dma** COF.[34] Thus, these proposed eclipsed AA packing models are subsequently used

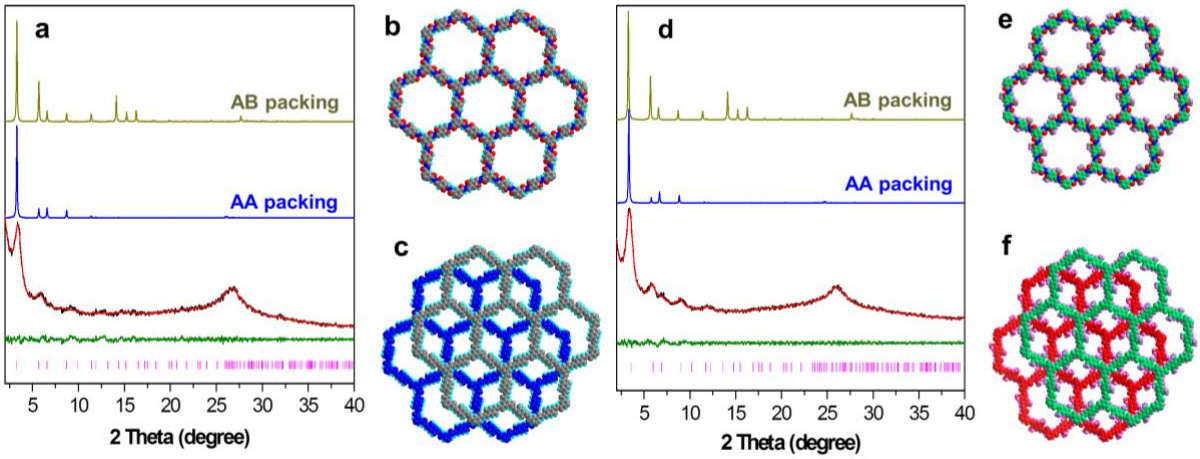

Figure 1. (**a**) Experimental (black), Pawley refined (red), their difference (green), simulated eclipsed AA stacking (blue) and staggered AB stacking (yellow) PXRD patterns of **Bth-Dha**. (**b, c**) Eclipsed AA and staggered AB packing structures of **Bth-Dha**. (**d**) Experimental (black), Pawley refined (red), their difference (green), simulated eclipsed AA stacking (blue) and staggered AB stacking (yellow) PXRD patterns of **Bth-Dma**. (**e, f**) Eclipsed AA and staggered AB packing structures of **Bth-Dma**. Bragg positions are indicated by pink ticks.

for the Pawley refinement, which create the PXRD patterns that are in good agreement with their corresponding experimental ones (Figure 1a and Figure 1d). The refinement results give rise to the following unit cell parameters: $a = b$ = 30.90 Å, c =3.41 Å for **Bth-Dha**, and $a = b$ = 30.72 Å, c = 3.75 Å for **Bth-Dma**, with the satisfactory agreement factors of R_p and R_{wp} being 4.87%, 6.32% for **Bth-Dha**, and 4.74%, 6.15% for **Bth-Dma**, respectively.

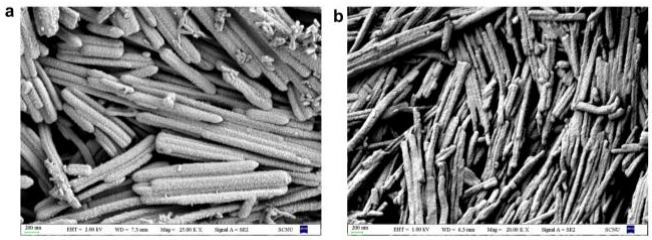

Figure 2. SEM images of **Bth-Dha** (**a**) and **Bth-Dma** (**b**) COFs.

To confirm the chemical composition of the as-prepared hydrazone-linked COFs, both Fourier transform infrared (FT-IR) and solid-state ^{13}C NMR spectroscopy were conducted. The characteristic bands of aldehyde C=O stretching vibrations for the starting materials of **Dha** and **Dma** disappear in the FT-IR spectra of **Bth-Dha** and **Bth-Dma**, implying that Schiff-base reactions occurred between the corresponding monomers (Figures S1-S2). The emerging peaks at 1615 and 1596 cm^{-1} can be observed in the FT-IR spectra of **Bth-Dha** and **Bth-Dma**, respectively, which are assignable to the characteristic C=N stretching vibrations of their hydrazone units.[35] Such characteristic bands of C=N group are close to that observed in the FT-IR spectrum of the **Tmt** model compound (1601 cm^{-1}). The ^{13}C cross-polarization magic-angle spinning (CP-MAS) solid-state NMR spectra exhibit characteristic signals for the expected C=N bonds of the hydrazone units at 150.3 and 150.8 ppm for **Bth-Dha** and **Bth-Dma**, respectively (Figures S3-S4). The signal of methyl group in the CP-MAS NMR spectrum of **Bth-Dma** appears at 55.7 ppm. Interestingly, the scanning electron microscopy (SEM) images of both **Bth-Dha** and **Bth-Dma** display well-defined nanorod shaped morphologies with average length being approximately 1 μm, as illustrated in Figure 2. In addition, both **Bth-Dha** and **Bth-Dma** display good thermal stability. As indicated by thermogravimetric analysis (TGA) conducted under air atmosphere, no significant weight loss is observed at temperatures below 320 ^{o}C (Figures S5-S6).

Nitrogen adsorption−desorption experiment was carried out to estimate the porous property of the as-prepared hydrazone-linked COFs. Prior to porosity measurement, the crystalline COFs were treated by Soxhlet extraction using THF as the solvent for 24 h, then heated at 120 ^{o}C for 10 h under a dynamic vacuum. As illustrated in Figure 3, the adsorption curves of **Bth-Dha** and **Bth-Dma** COFs show nitrogen uptakes in the low relative pressures range (P/P_0 = 0−0.01), indicating both of them are porous materials. When utilizing the Brunauer–Emmett–Teller (BET) model in the scope of P/P_0 between 0.05 and 0.25 (Figures S7-S8), specific surface areas of 130 $m^2 g^{-1}$ for **Bth-Dha** and 392 $m^2 g^{-1}$ for **Bth-Dma** can be obtained. On the basis of a single point measurement at P/P_0 = 0.99, their total pore volumes are determined to be 0.22 and 0.44 $cm^3 g^{-1}$ for **Bth-Dha** and **Bth-Dma**, respectively. In addition, the pore size distributions of **Bth-Dha** and **Bth-Dma** COFs are evaluated *via* non-local density functional theory (NLDFT) employing the carbon cylindrical pore adsorption branch mode. As presented in Figure 3, both the **Bth-Dha** and **Bth-Dma** COFs display narrow pore size distributions with the main peaks being around 1.9 and 1.7 nm, respectively, both of which are smaller than those of the theoretical pore sizes estimated from their corresponding AA packing structures. Such relatively low BET surface areas and slight deviations of the pore size distributions of **Bth-Dha** and **Bth-Dma** COFs are probably due to the difficulty in removal of part of guest solvents and/or unreacted monomers, which occupy the pore channels of the corresponding frameworks due to hydrogen-bonding interactions.[34, 36]

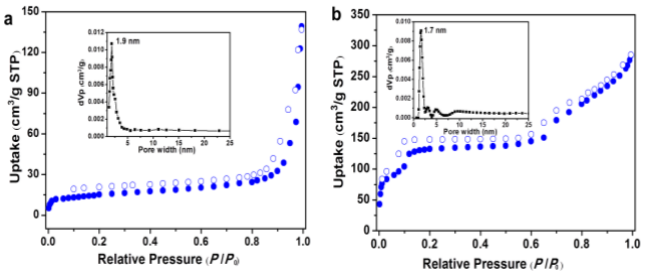

Figure 3. N_2 adsorption and desorption isotherm curves (77 K) of **Bth-Dha** (**a**) and **Bth-Dma** (**b**). Inset: their corresponding pore size distribution profiles.

The chemical stabilities of the hydrazone-linked **Bth-Dha** and **Bth-Dma** COFs were further explored by soaking the as-prepared crystalline samples for 24 h in a variety of solvents including H_2O, THF, EtOH, hexane (Hex) and DMF at room temperature. No decomposition of the **Bth-Dha** and **Bth-Dma** COF samples could be observed after all the treatments. The solvent-treated samples were isolated, dried and subjected to PXRD measurement again. As presented in Figure 4, the PXRD measurements suggest that the crystallinities of both **Bth-Dha** and **Bth-Dma** COFs are retained upon treatment of different solvents, confirming the high chemical stabilities of the resulting hydrazone-linked COFs. The excellent thermal and chemical stabilities of **Bth-Dha** and **Bth-Dma** COFs may be attributed to the more robust hydrazone linkages in the frameworks. [37]

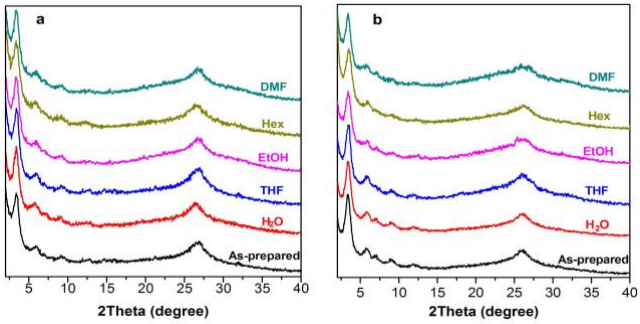

Figure 4. PXRD patterns of **Bth-Dha** (**a**) and **Bth-Dma** (**b**) after treatment for 24 h in different solvents at room temperature.

Previous studies have shown that some of the hydrazone-linked COFs exhibit outstanding photoluminescent properties[24,34]. Thus, the photoluminescent properties of both **Bth-Dha** and **Bth-Dma** COFs have been investigated in the solid state at room temperature. The powder of **Bth-Dma** displays quite strong fluorescence, while the **Bth-Dha** COF and the model compound **Tmt** are almost non-emissive under our experimental conditions. As described in Figure S9, **Bth-Dma** COF shows photoluminescence in the solid state with maximum emission wavelength at 542 nm (λ_{ex} = 375 nm). When dispersed in pure water, **Bth-Dma** COF still presents intense fluorescence but showing maximum emission at 518 nm upon excitation at 393 nm (Figure S10). The fluorescence in Bth-Dma can be attributed to the restricted intramolecular bond rotation,[34] while the non-emissive behavior of Bth-Dha is presumably related to non-radiative decay through excited state proton transfer involving the active phenol protons.[38] The metal cation sensing studies were then conducted by addition of the corresponding chloride salts to **Bth-Dma** COF suspensions, with the concentration of the metal ions being 100 μM. Corresponding 5b, the emission intensity of **Bth-Dma** COF suspension progressively decreases with the increasing concentration of Fe^{3+} ions from 0 to 100 μM. Such a fluorescence quenching effect can be clearly observed under a portable UV lamp (with λ_{ex} = 365 nm), showing obvious intensity change (inset photo in Figure 5b). In the low Fe^{3+} concentration range, a linear Stern–Volmer relationship is observed, from which a quenching constant (K_{sv}) value of 2.3×10^4 M^{-1} (Figure S12) can be obtained, which is comparable to those of the COF or MOF-type materials for detection of Fe^{3+} ion.[26,39,40] The detection limit for Fe^{3+} ion is calculated to be 0.17 μM (Figure S13), demonstrating the high selectivity toward Fe^{3+}. The effects of pH and counter anions on the fluorescence of **Bth-Dma** were also investigated. As indicated in Figure S14 and S15, neither pH (in the range between 4 and 10) nor anions (Cl^-, Br^-, NO_3^-, and OAc^-) has an impact on the fluorescence quenching efficiency, suggesting that the selective Fe(III) sensing is barely affected by pH and anions.

Since abundant *O,N,O'*-chelating sites are embedded in the pore wall structure of **Bth-Dma** COF, it is postulated that the recognition process is due to the effective coordination of Fe(III)

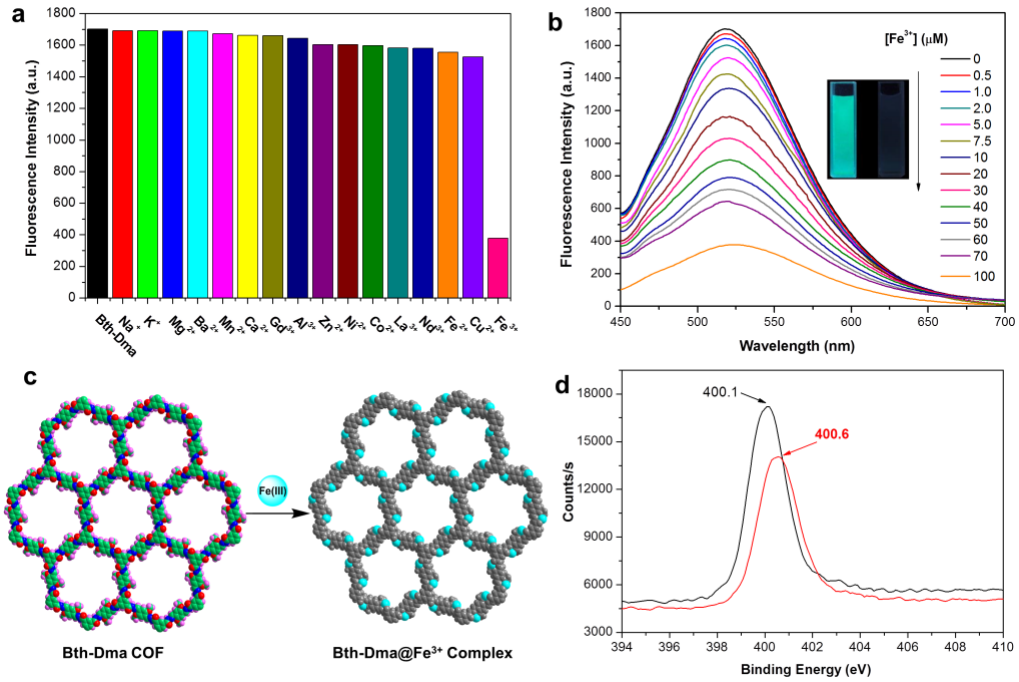

Figure 5. (**a**) Comparison of the luminescence intensity of **Bth-Dma** COF in the presence of various metal ions (100 μM) in water (λ_{ex} = 393 nm). (**b**) Emission spectra of **Bth-Dma** COF in water suspensions containing various $C_{Fe^{3+}}$ (0 to 100 μM). Inset: a photo showing fluorescence change (under a UV lamp with λ_{ex} = 365 nm) of **Bth-Dma** COF in water upon addition of 100 μM of Fe^{3+} ion. (**c**) Schematic illustration of the proposed sensing mechanism of **Bth-Dma** COF towards Fe^{3+} ion. (**d**) N1s XPS spectra of the **Bth-Dma** COF (black) and the **Bth-Dma@Fe^{3+}** complex (red).

emission spectra of the suspensions indicate that the luminescence intensity of **Bth-Dma** is largely dependent on the species of metal ions (Figure 5a). Addition of metal cations such as Na^+, K^+, Mg^{2+}, Ba^{2+}, Mn^{2+}, Ca^{2+}, Gd^{3+} or Al^{3+} to the suspensions leads to almost no change on the luminescence intensity of **Bth-Dma** COF, while addition of Zn^{2+}, Ni^{2+}, Co^{2+}, La^{3+}, Nd^{3+}, Fe^{2+} or Cu^{2+} only result in a slight decrease in its luminescence intensity. In contrast, the luminescence intensity of **Bth-Dma** COF is significantly quenched upon the addition of Fe^{3+} cation (Figure S11). These results suggest that **Bth-Dma** COF may be used as a chemical sensor for detecting Fe^{3+} *via* luminescence quenching. To better understand the sensing ability of **Bth-Dma** towards Fe^{3+} ion, a fluorescence titration experiment was performed by following the spectroscopic changes upon the addition of Fe^{3+} to **Bth-Dma** COF. As shown in Figure ion with the *O,N,O'*-chelating sites (Figure 5c), which affects fluorescence quenching through energy or electron transfer with excited states involving d-orbital electrons.[30] To further support the proposed possible mechanism of recognition process, the **Bth-Dma@Fe^{3+}** complex was synthesized by soaking the **Bth-Dma** COF powder (10 mg) in the $FeCl_3$ aqueous solution (100 μM, 200 mL) for two days at room temperature. The resulting **Bth-Dma@Fe^{3+}** complex was collected by centrifugation, washed with water and THF thoroughly, and then subjected to PXRD and X-ray photoelectron spectroscopy (XPS) measurements. As described in Figure S16, the PXRD pattern of the obtained **Bth-Dma@Fe^{3+}** complex is very similar to that of the parent **Bth-Dma** COF, indicating the 2D COF structure is retained. Furthermore, Fe2p XPS of the **Bth-Dma@Fe^{3+}** complex (Figure S17) exhibits two

peaks at 711.4 and 724.8 eV, which can be ascribed to the $Fe2p_{3/2}$ and $Fe2p_{1/2}$ binding energies,[41] respectively, further confirming the successful immobilization of Fe^{3+} ion within the pore channels of **Bth-Dma** COF. Moreover, the N1s peak from the hydrazone units of the **Bth-Dma** COF shifted from 400.1 eV[42] to 400.6 eV when the Fe^{3+} ion is added (Figure 5d), again supporting the binding event between the *O*,*N*,*O'*-chelating sites and Fe(III) ion in the resulting **Bth-Dma@Fe^{3+}** complex.[43] The loading capacity of Fe^{3+} within **Bth-Dma** was evaluated by measuring the concentration of Fe^{3+} before and after treatment with **Bth-Dma**, as determined using UV-vis spectroscopy (Figure S18). The amount of the $FeCl_3$ loading on **Bth-Dma** COF is calculated to be around 11.9 wt%, which amounts to ~1.6 Fe per pore. The particle-size distribution of the **Bth-Dma** COF before and after addition of Fe^{3+} was measured by dynamic light scattering (DLS), indicating an increase of the average particle size from 308 to 394 nm (Figure S19). This change may be attributed to the slight increase of hydrodynamic diameter of the COF aggregates due to the immobilization of Fe^{3+}. The Fe^{3+}-ligand coordination interaction is further verified through the ^{1}H NMR study of the binding between Fe^{3+} and the model compound **Tmt**. As described in Figure S20, upon the addition of 3 equiv. Fe^{3+} cation into the DMSO-d_6 solution of **Tmt**, the ^{1}H NMR resonances of the hydrogen atoms from the hydrazone and phenyl groups are all significantly shifted to lower frequencies compared with those of free **Tmt**, corresponding to the coordination interaction between Fe(III) ion and the **Tmt** model compound.

CONCLUSIONS

In summary, we have rationally designed and successfully prepared two hydrazone-linked COFs including **Bth-Dha** and **Bth-Dma** with functional *O*,*N*,*O'*-chelating sites. The obtained hydrazone-linked COFs exhibit good crystallinity, moderate surface area and excellent thermal and chemical stability. More interestingly, the as-synthesized **Bth-Dma** COF displays strong fluorescence in both the solid state and aqueous suspension, and exhibits a highly selective and sensitive luminescence response toward Fe^{3+} in water, indicating its potential as a fluorescence sensor for detection of Fe^{3+} ion. The good selectivity and sensitivity can be assigned to the favorable coordination interaction between Fe(III) ion and the *O*,*N*,*O'*-chelating sites in the pore wall of **Bth-Dma** COF, which has been proven by X-ray photoelectron spectroscopy and ^{1}H NMR results. To the best of our knowledge, this represents the first example of detecting Fe(III) ion using a robust luminescent COF material containing predesigned *O*,*N*,*O'*-chelating sites, which paves the way for the design of selective fluorescent COF sensors towards different metal ions.

ASSOCIATED CONTENT

Supporting Information. FT-IR spectra, NMR spectra, TGA curves, PXRD, XPS, additional fluorescence spectra, tables for the fractional atomic coordinates of the simulated COFs. This material is available free of charge *via* the Internet at http://pubs.acs.org.

AUTHOR INFORMATION

Corresponding Author

songliangcai@m.scnu.edu.cn; wgzhang@scnu.edu.cn; yliu@lbl.gov

Notes

The authors declare no competing financial interest.

ACKNOWLEDGMENT

We gratefully acknowledge the financial support from the National Natural Science Foundation of P. R. China (Grant Nos. 21603076, 21473062 and 21571070), the Natural Science Foundation of Guangdong Province (Grant Nos. 2016A030310437 and 2018A030313193), and the Undergraduates' Innovating Experimentation Project of SCNU and Guangdong Province (Grant No. 20181462). Part of this work was performed as a user project at the Molecular Foundry, Lawrence Berkeley National Laboratory, supported by the Office of Science, Office of Basic Energy Sciences, of the U. S. Department of Energy under Contract No. DE-AC02-05CH11231.

REFERENCES

(1) Cote, A. P.; Benin, A. I.; Ockwig, N. W.; O'Keeffe, M.; Matzger, A. J.; Yaghi, O. M. Porous, Crystalline, Covalent Organic Frameworks. *Science* **2005**, 310, 1166-1170.

(2) Diercks, C. S.; Yaghi, O. M. The Atom, the Molecule, and the Covalent Organic Framework. *Science* **2017**, 355, eaal1585.

(3) Cai, S. L.; Zhang, W. G.; Zuckermann, R. N.; Li, Z. T.; Zhao, X.; Liu, Y. The Organic Flatland-Recent Advances in Synthetic 2D Organic Layers. *Adv. Mater.* **2015**, 27, 5762-5770.

(4) Segura, J. L.; Mancheno, M. J.; Zamora, F. Covalent Organic Frameworks Based on Schiff-Base Chemistry: Synthesis, Properties and Potential Applications. *Chem. Soc. Rev.* **2016**, 45, 5635-5671.

(5) Li, X. L.; Zhang, C. L.; Cai, S. L.; Lei, X. H.; Altoe, V.; Hong, F.; Urban, J. J.; Ciston, J.; Chan, E. M.; Liu, Y. Facile Transformation of Imine Covalent Organic Frameworks into Ultrastable Crystalline Porous Aromatic Frameworks. *Nat. Commun.* **2018**, 9, 2998.

(6) Doonan, C. J.; Tranchemontagne, D. J.; Glover, T. G.; Hunt, J. R.; Yaghi, O. M. Exceptional Ammonia Uptake by a Covalent Organic Framework. *Nat. Chem.* **2010**, 2, 235-238.

(7) Zhang, Y. B.; Su, J.; Furukawa, H.; Yun, Y.; Gandara, F.; Duong, A.; Zou, X.; Yaghi, O. M. Single-Crystal Structure of a Covalent Organic Framework. *J. Am. Chem. Soc.* **2013**, 135, 16336-16339.

(8) Kang, Z.; Peng, Y.; Qian, Y.; Yuan, D.; Addicoat, M. A.; Heine, T.; Hu, Z.; Tee, L.; Guo, Z.; Zhao, D. Mixed Matrix Membranes (MMMs) Comprising Exfoliated 2D Covalent Organic Frameworks (COFs) for Efficient CO_2 Separation. *Chem. Mater.* **2016**, 28, 1277-1285.

(9) Fang, Q. R.; Wang, J. H.; Gu, S.; Kaspar, R. B.; Zhuang, Z. B.; Zheng, J.; Guo, H. X.; Qiu, S. L.; Yan, Y. S. 3D Porous Crystalline Polyimide Covalent Organic Frameworks for Drug Delivery. *J. Am. Chem. Soc.* **2015**, 137, 8352–8355.

(10) Bai, L. Y.; Phua, S. Z. F.; Lim, W. Q.; Jana, A.; Luo, Z.; Tham, H. P.; Zhao, L. Z.; Gao, Q.; Zhao, Y. L. Nanoscale Covalent Organic Frameworks as Smart Carriers for Drug Delivery. *Chem. Commun.* **2016**, 52, 4128–4131.

(11) Vyas, V. S.; Vishwakarma, M.; Moudrakovski, I.; Haase, F.; Savasci, G.; Ochsenfeld, C.; Spatz, J. P.; Lotsch, B. V. Exploiting Noncovalent Interactions in an Imine-Based Covalent Organic Framework for Quercetin Delivery. *Adv. Mater.* **2016**, 28, 8749–8754.

(12) Ding, S. Y.; Gao, J.; Wang, Q.; Zhang, Y.; Song, W. G.; Su, C. Y.; Wang, W. Construction of Covalent Organic Framework for Catalysis: Pd/COF-LZU1 in SuzukiMiyaura Coupling Reaction. *J. Am. Chem. Soc.* **2011**, 133, 19816–19822.

(13) Han, X.; Xia, Q.; Huang, J.; Liu, Y.; Tan, C.; Cui, Y. Chiral Covalent Organic Frameworks with High Chemical Stability for Heterogeneous Asymmetric Catalysis. *J. Am. Chem. Soc.* **2017**, 139, 8693–8697.

(14) Zhang, J.; Han, X.; Wu, X. W.; Liu, Y., Cui, Y. Multivariate Chiral Covalent Organic Frameworks with Controlled Crystallinity and Stability for Asymmetric Catalysis. *J. Am. Chem. Soc.* **2017**, 139, 8277–8285.

(15) Ma, H. P.; Liu, B. L.; Zhang, L. M.; Li, Y. G.; Tan, H. Q.; Zang, H. Y.; Zhu, G. S. Cationic Covalent Organic Frameworks: a Simple Platform of Anionic Exchange for Porosity Tuning and Proton Conduction. *J. Am. Chem. Soc.* **2016**, 138, 5897–5903.

(16) Cai, S. L.; Zhang, Y. B.; Pun, A. B.; He, B.; Yang, J.; Toma, F. M.; Sharp, I. D.; Taghi, O. M.; Fan, J.; Zheng, S. R.; Zhang, W. G.; Liu, Y. Tunable Electrical Conductivity in Oriented Thin Films of Tetrathiafulvalene-Based Covalent Organic Framework. *Chem. Sci.* **2014**, 5, 4693–4700.
(17) Medina, D. D.; Petrus, M L.; Jumabekov, A. N.; Margraf, J. T.; Weinberger, S.; Rotter, J. M.; Clark, T. C.; Bein, T. Directional Charge-Carrier Transport in Oriented Benzodithiophene Covalent Organic Framework Thin Films. *ACS Nano* **2017**, 11, 2706–2713.
(18) Xue, R.; Guo, H.; Wang, T.; Gong, L.; Wang, Y. N.; Ai, J. B.; Huang, D. D.; Chen, H. Q.; Yang, W. Fluorescence Properties and Analytical Applications of Covalent Organic Frameworks, *Anal. Methods* **2017**, 9, 3737–3750.
(19) Kreno, L. E.; Leong, K.; Farha, O. K.; Allendorf, M.; Van Duyne, R. P.; Hupp, J. T. Metal-Organic Framework Materials as Chemical Sensors. *Chem. Rev.* **2012**, 112, 1105-1125.
(20) Hu, Z.; Deibert, B. J.; Li, J. Luminescent Metal-Organic Frameworks for Chemical Sensing and Explosive Detection. *Chem. Soc. Rev.* **2014**, 43, 5815-5840.
(21) Dalapati, S.; Jin, S.; Gao, J.; Xu, Y.; Nagai, A.; Jiang, D. An Azine-Linked Covalent Organic Framework. *J. Am. Chem. Soc.* **2013**, 135, 17310-17313.
(22) Lin, G.; Ding, H.; Yuan, D.; Wang, B.; Wang, C. A Pyrene-Based, Fluorescent Three-Dimensional Covalent Organic Framework. *J. Am. Chem. Soc.* **2016**, 138, 3302-3305.
(23) Zhu, M. W.; Xu, S.; Wang, X.; Chen, Y.; Dai, L.; Zhao, X. The Construction of Fluorescent Heteropore Covalent Organic Frameworks and Their Applications in Spectroscopic and Visual Detection of Trinitrophenol with High Selectivity and Sensitivity. *Chem. Commun.* **2018**, 54, 2308-2311.
(24) Ding, S. Y.; Dong, M.; Wang, Y. W.; Chen, Y. T.; Wang, H. Z.; Su, C. Y.; Wang, W. A Thioether-Based Fluorescent Covalent Organic Framework for Selective Detection and Facile Removal of Mercury(II). *J. Am. Chem. Soc.* **2016**, 138, 3031-3037.
(25) Li, Z.; Zhang, Y.; Xia, H.; Mu, Y.; Liu, X. A Robust and Luminescent Covalent Organic Framework as a Highly Sensitive and Selective Sensor for the Detection of Cu^{2+} Ions. *Chem. Commun.* **2016**, 52, 6613-6616.
(26) Wang, L. L.; Yang, C. X.; Yan, X. P. Exploring Fluorescent Covalent Organic Frameworks for Selective Sensing of Fe^{3+}. *Sci. China Chem.* **2018**, 61, 1470-1474.
(27) Peng, Y. W.; Huang, Y.;; Zhu, Y. H.; Chen, B.; Wang, L. Y.; Lai, Z. C.; Zhang, Z. C.; Zhao, M. T.; Tan, C. L.; Yang, N. L.; Shao, F. W.; Han, Y.; Zhang, H. Ultrathin Two-Dimensional Covalent Organic Framework Nanosheets: Preparation and Application in Highly Sensitive and Selective DNA Detection. *J. Am. Chem. Soc.* **2017**, 139, 8698-8704.
(28) Sahoo, S. K.; Sharma, D.; Bera, R. K.; Crisponi, G.; Callan, H. F. Iron(III) Selective Molecular and Supramolecular Fluorescent Probes. *Chem. Soc. Rev.* **2012**, 41, 7195-7227.
(29) Zhang, C.; Yan, Y.; Pan, Q.; Sun, L.; He, H.; Liu, Y.; Liang, Z.; Li, J. A Microporous Lanthanum Metal-Organic Framework as a Bi-Functional Chemosensor for the Detection of Picric Acid and Fe^{3+} Ions. *Dalton. Trans.* **2015**, 44, 13340-13346.
(30) Zheng, M.; Tan, H.; Xie, Z.; Zhang, L.; Jing, X.; Sun, Z. Fast Response and High Sensitivity Europium Metal Organic Framework Fluorescent Probe with Chelating Terpyridine Sites for Fe^{3+}. *ACS Appl. Mater. Inter.* **2013**, 5, 1078-1083.
(31) Chen, C. H.; Wang, X. S.; Li, L.; Huang, Y. B.; Cao, R. Highly Selective Sensing of Fe^{3+} by an Anionic Metal-Organic Framework Containing Uncoordinated Nitrogen and Carboxylate Oxygen Sites. *Dalton. Trans.* **2018**, 47, 3452-3458.
(32) Aruffo, A. A.; Murphy, T. B.; Johnson, D. K.; Rose, N. J.; Schomaker, V. Structural Studies of Fe(III) and Cu(II) Complexes of Salycylaldehyde Benzoyl Hydrazone, a Synthetic Chelating Agent Exhibiting Diverse Biological Properties. *Inorg.Chim. Acta* **1982**, 67, L25-L27.
(33) Yang, C. C.; Hsu, C. J.; Chou, P. T.; Cheng, H. C.; Su, Y. O.; Leung, M. K. Excited State Luminescence of Multi-(5-phenyl-1,3,4-oxadiazo-2-yl)benzenes in an Electron-Donating Matrix: Exciplex or Electroplex? *J. Phys. Chem. B* **2010**, 114, 756-768.
(34) Li, X.; Gao, Q.; Wang, J.; Chen, Y.; Chen, Z. H.; Xu, H. S.; Tang, W.; Leng, K.; Ning, G. H.; Wu, J.; Xu, Q. H.; Quek, S. Y.; Lu, Y.; Loh, K. P. Tuneable Near White-Emissive Two-Dimensional Covalent Organic Frameworks. *Nat. Commun.* **2018**, 9, 2335.
(35) Zhang, K.; Cai, S. L.; Yan, Y. L.; He, Z. H.; Lin, H. M.; Huang, X. L.; Zheng, S. R.; Fan, J.; Zhang, W. G. Construction of a Hydrazone-Linked Chiral Covalent Organic Framework-Silica Composite as the Stationary Phase for High Performance Liquid Chromatography. *J. Chromatogr. A* **2017**, 1519, 100-109.
(36) Wang, X.; Han, X.; Zhang, J.; Wu, X.; Liu, Y.; Cui, Y. Homochiral 2D Porous Covalent Organic Frameworks for Heterogeneous Asymmetric Catalysis. *J. Am. Chem. Soc.* **2016**, 138, 12332-12335.
(37) Uribe-Romo, F. J.; Doonan, C. J.; Furukawa, H.; Oisaki, K.; Yaghi, O. M. Crystalline Covalent Organic Frameworks with Hydrazone Linkages. *J. Am. Chem. Soc.* **2011**, 133, 11478-11481.
(38) Zhao, J. Z.; Ji, S. M.; Chen, Y. H.; Guo, H. M.; Yang, P. Excited State Intramolecular Proton Transfer (ESIPT): From Principal Photophysics to the Development of New Chromophores and Applications in Fluorescent Molecular Probes and Luminescent Materials. *Phys. Chem. Chem. Phys.*, **2012**, 14, 8803-8817.
(39) Li, L.; Shen, S.; Ai, W.; Song, S.; Bai, Y.; Liu, H. Facilely Synthesized Eu^{3+} Post-Functionalized UiO-66-Type Metal-Organic Framework for Rapid and Highly Selective Detection of Fe^{3+} in Aqueous Solution. *Sensor Actuat. B: Chem.* **2018**, 267, 542-548.
(40) Arici, M. Luminescent 2D + 2D → 2D Interpenetrated Zn(II)-Coordination Polymer Based on Reduced Schiff Base Tricarboxylic Acid and Bis(imidazole) Ligand for Detection of Picric Acid and Fe^{3+} Ions. *Cryst. Growth Des.* **2017,** 17, 5499-5505.
(41) Xu, Z.; Yu, J. Visible-Light-Induced Photoelectrochemical Behaviors of Fe-Modified TiO_2 Nanotube Arrays. *Nanoscale* **2011**, 3, 3138-3144.
(42) Wu, M. X.; Chen, G.; Liu, P.; Zhou, W. H.; Jia, Q. Polydopamine-Based Immobilization of a Hydrazone Covalent Organic Framework for Headspace Solid-Phase Microextraction of Pyrethroidsin Vegetables and Fruits. *J. Chromatogr. A* **2016,** 1456, 34-41.
(43) Chen, B.; Wang, L.; Xiao, Y.; Fronczek, F. R.; Xue, M.; Cui, Y.; Qian, G. A Luminescent Metal-Organic Framework with Lewis Basic Pyridyl Sites for the Sensing of Metal Ions. *Angew. Chem. Int. Ed.* **2009,** 48, 500-503.

Table of Contents

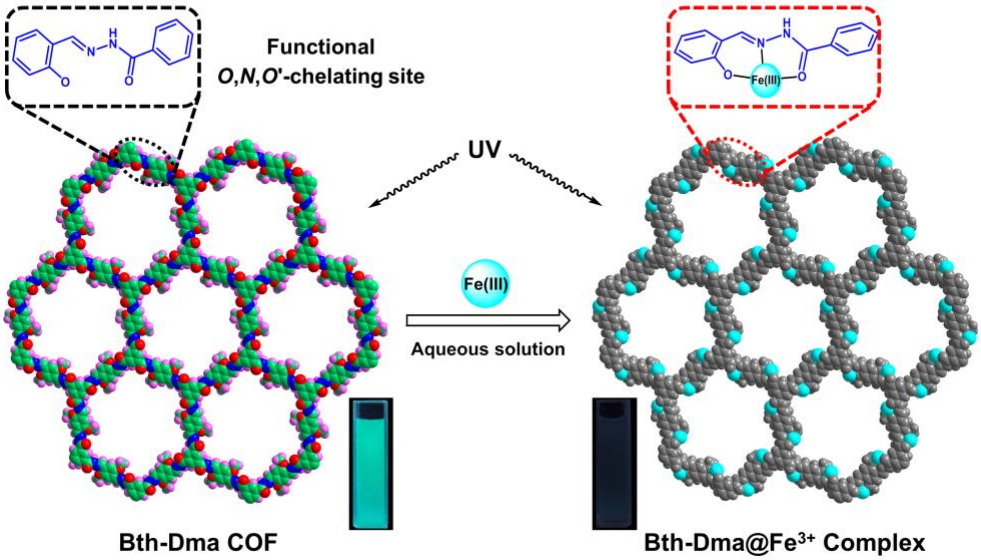
Functional
O,N,O'-chelating site
UV
Fe(III)
Aqueous solution
Bth-Dma COF
Bth-Dma@Fe3+ Complex